Efficiency simulations of the nEDM@SNS light collection system

Devon Loomis,[1,*] Vince Cianciolo,[2] and Jed Leggett[3]

[1] *Western Kentucky University, Bowling Green, KY 42101, USA*
[2] *Physics Division, Oak Ridge National Laboratory, Oak Ridge, TN 37830, USA*
[3] *Mississippi State University, Mississippi State, MS 39762, USA*

(Dated: January 20, 2021)

A system for collecting the scintillation light produced by the capture process of ultra-cold neutrons (UCN) on polarized ^{3}He is discussed and results from simulations validating its performance are presented. This system will be implemented in nEDM@SNS, the experiment searching for the neutron electric dipole moment (nEDM) at the Spallation Neutron Source (SNS) at Oak Ridge National Laboratory. Simulated results show that the light collection system collects on average $\sim$16.5 photoelectrons per UCN-^{3}He capture event (sufficient to generate a robust signal), reconstructs the event location in the beam direction with $\sim$3 cm accuracy, and detects capture events and the correlated β decay background with uniform ($\delta\epsilon < 2\%$) spatial efficiency.

Keywords: Neutron EDM, Ultracold Neutrons

I. INTRODUCTION

The presence of a nonzero permanent neutron electric dipole moment (nEDM), a measure of the charge distribution within the neutron, would be a violation of both parity (P) and time reversal (T) invariance and a clear signature of physics beyond the standard model. The nEDM@SNS experiment [1] will utilize the technique introduced by Golub and Lamoreaux [2] to measure the nEDM with a two order of magnitude improvement of sensitivity over recent nEDM measurements [3]. Neutrons with de Broglie wavelength $\lambda = 8.9$Å (kinetic energy = 1 meV) from the Fundamental Neutron Physics Beamline at the SNS of ORNL are directed into two measurement cells filled with superfluid ^{4}He and a dilute concentration of polarized ^{3}He. The superfluid ^{4}He downscatters a fraction of the incoming neutrons to energies low enough that they can be trapped within the measurement cells. These "ultracold neutrons" (UCN) can be stored in the measurement cells for long periods (hundreds of seconds), maximizing observation time and increasing sensitivity. In a magnetic field, both the UCN and ^{3}He precess with similar gyromagnetic ratios. The UCN-^{3}He capture process

$$n + {}^3He \rightarrow p + {}^3H + 764\,\text{keV} \tag{1}$$

deposits 764 keV of kinetic energy into the superfluid ^{4}He, which in turn produces a burst of extreme ultraviolet (EUV) scintillation light (80 nm) [4–6]. The capture process is strongly spin-dependent. As a result, the scintillation rate will vary with frequency equal to the difference between UCN and ^{3}He precession frequencies.

The nEDM can be extracted with two different measurement techniques that look for a linear shift in the neutron precession frequency. The free precession technique measures the frequency shift upon a reversal of an electric field relative to the magnetic field. Alternatively, the critical spin dressing technique applies an alternating magnetic field, driving the ^{3}He and UCN to precess at the same frequency unless a nonzero nEDM introduces a time dependent shift. These measurement techniques are discussed in greater depth in [1].

To measure the scintillation signal from UCN-^{3}He capture, a light collection system, composed of wavelength-shifting optical fibers, an array of silicon photomultipliers (SiPM's), a wavelength-shifting coating, and a thin dielectric reflector (a more thorough description of the system is offered in Sec. II), has been designed specifically in accordance with the relevant design requirements of the experiment. Many design choices have been made prior to this study with these constraints in mind. For instance, due to mechanical considerations in the experiment's central detecting apparatus and measurement cells, the system was chosen to be fiber-based and, given the emission spectrum of the wavelength-shifting coating, Kuraray Y-11 fibers were selected. The electrostatic requirements of the system constrain the fiber placement to be adjacent to the ground electrode of the high voltage system. The readout architecture achieves the required high photoelectron detection efficiency (PDE) and dark rate suppression by using an array of small area cooled SiPMs.

The simulation study at hand was undertaken to address the impact of design parameters that still remain in question and can be resolved from a Monte Carlo approach. These parameters include fiber dye density, diameter, and length, fiber embedding in the measurement cell walls, and dielectric reflector surface roughness. With these parameters addressed, we then proceed to a full capture event simulation in which we resolve the light collection system's event detection and

* Email: devon.loomis958@topper.wku.edu

beta decay background rejection efficiencies, as well as event position reconstruction capabilities. In Sec. II we discuss the light collection apparatus in more detail, and the simulation framework used in this study. In Sec. III, we discuss results from simulations, in particular showing the efficiency of signal detection among a beta decay-dominated background. Finally, in Sec. IV we present conclusions and discuss future implementations/studies of the light collection system.

II. APPARATUS AND PROCEDURE

A. Light collection apparatus

The light collection system, located inside the experiment's central volume (Fig. 1) with the measurement cells and high voltage electrodes, is responsible for transporting the scintillation light from the UCN-^{3}He capture events to the readout electronics located exterior to the volume.

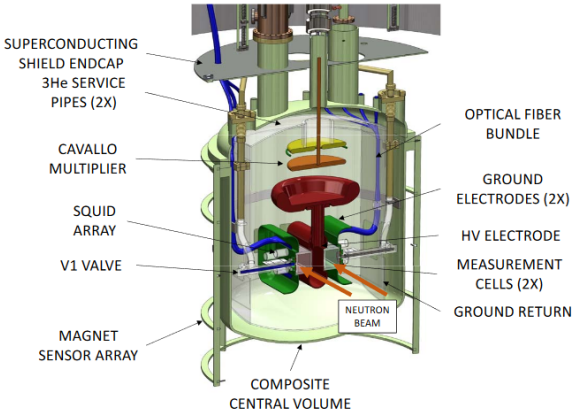

Figure 1. Central volume of the nEDM@SNS experiment [1].

EUV photons have short absorption lengths in nearly all materials other than helium, so they must be converted into optical wavelengths by a wavelength-shifting coating on the measurement cell walls. A coating made by dissolving deuterated tetraphenyl butadiene (dTPB) [9–11] and deuterated polystyrene (dPS) [12] in deuterated toluene has been shown to retain the ^{3}He polarization [13] and neutron density [14] for times that are long relative to the neutron β-decay lifetime. Some of the photons that enter the dTPB coating as EUV photons are converted to blue wavelengths and collected by Kuraray Y-11 wavelength-shifting fibers pressed against the measurement cell wall near the ground electrode (Fig. 2). To prevent a substantial number of photons escaping from the measurement cell before reaching the optical fibers, a thin specular reflector dielectric film made of Vikuiti VM2000 will be placed on the other cell walls.

Once in the fibers, the photons are converted to green wavelengths and transported to the surface of the central volume where they are mated to clear fibers that lead to an array of silicon photomultipliers (SiPMs) placed outside due to the magnetic properties of the readout electronics. Hamamatsu 13360-75 SiPMs [7] were selected for their high photon detection efficiency (PDE) and because they are well characterized at low temperatures [8]. Operating these sensors at (insert temp here), reduces the dark rate substantially, preventing a significant concealment of signal afterpulses. Additionally, the dark rate is suppressed by choosing small area SiPM's that are tuned to the fiber diameter. Previous calculations have shown that the fiber length contribution to dark rate is minimal [??].

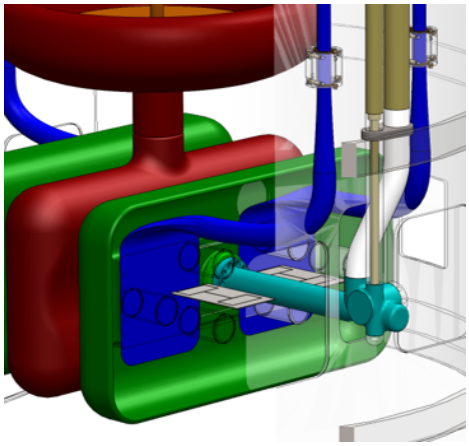

Figure 2. Wavelength-shifting fibers (blue) attached to the ground electrode side (green) of the measurement cell walls.

A photon counting technique [1], in which any SiPM detection is assumed to correspond to a single photon, is implemented by discriminating each analog SiPM readout at ~ 0.5 per photoelectron to create a digital signal. With this technique, we can record the arrival time of each photon, enabling pulse-shape discrimination by analyzing the events in different time windows. Additionally, this technique minimizes optical cross talk while the SiPMs are operated at a relatively high overvoltage (8 V above the breakdown voltage V_{BR} where signals begin). At this operating voltage, the PDE (Fig. 3) is maximized ($\sim$ 1.3 times greater than standard operating voltage) and its dependence on voltage, temperature, and sensor variation is minimized [8]. Any gain dependence on voltage, temperature, and sensor variation is eliminated by using a digital output. The number of photons that can be extracted for a signal event in the experiment is limited. This, the PDE loss suffered when multiple photons from the same event hit

the same SiPM is only a few percent.

B. Simulation procedure

To quantify the expected light collection and event detection efficiency, as well as investigate the effects of some system parameters, GEANT4 was used to track photons from UCN-3He capture event emission until they are wavelength-shifted in the fibers. We avoid simulating the transmission of fibers and detection in the SiPMs by applying an ad hoc transmission probability and detection probability.

GEANT4 was a natural fit for the Light Collection simulation because of its thorough treatment of optical physics and material properties [15]. The simulation is constructed as follows: 80 nm photons are emitted uniformly in the superfluid ^{4}He of a measurement cell. They travel through the helium until reaching the dTPB layer on the measurement cell wall, which absorbs and re-emits 33% of the photons wavelength-shifted in a spectrum centered around 450 nm [16]. The photons then travel through the acrylic with a small chance of absorbing before reaching the optical fibers, where they are collected, wavelength-shifted corresponding to the emission spectrum of Kuraray Y-11 fibers with 1.5 m length (Fig. 3), and then killed by the simulation. For those photons that do not head directly towards the optical fibers, a Vikuiti dielectric mirror (96% reflectivity [17]) surface is installed on the other cell wall surfaces to prevent photons from escaping the measurement cell.

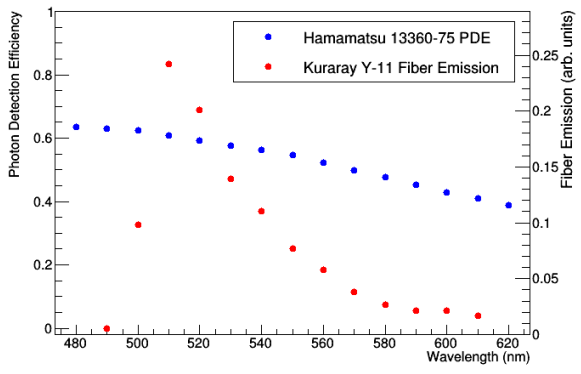

Figure 3. Photon detection efficiency vs wavelength (PDE(λ)) of a Hamamatsu 13360-75 SiPM at $V_{BR} + 8V$ and the emission spectrum for Kuraray Y-11 optical fibers at 1.5 m.

The efficiency of detecting photons that are wavelength-shifted by the fibers is determined by accounting for the Y-11 fiber trapping efficiency [18], transmission losses in the Y-11 [19] and clear fibers [20], and losses from fiber transitions and bends. The efficiencies associated with the transport of the photons from the fibers to the SiPMs are given in Table I.

Efficiencies	
Fiber trapping	10%
Fiber transmission	42%
Fiber-to-fiber	90%
Fiber-to-SiPM	90%
Fiber bends	95%

Table I. Efficiencies of mechanisms for transporting photons through fibers

The photons are tracked through the process of wavelength shifting in the dTPB, transmission in the acrylic and wavelength-shifting in the fibers. If successfully wavelength-shifted in the fibers, we sample a uniform random number, compare it to $1 - \text{PDE}(\lambda)$ at the collected photon's wavelength, and count a detected photoelectron if the sampled random number is greater. The photon counting technique outlined in II A is then accounted for by limiting to one photon count per event in any individual SiPM.

III. RESULTS AND DISCUSSION

A. Parametric studies

Before capture events were systematically studied in GEANT4, preliminary simulations were performed to find parametric effects from the optical fibers, dTPB, and Vikuiti VM2000 dielectric film. We use the fiber collection efficiency i.e., the fraction of photons that are successfully wavelength-shifted in the fibers, as the metric for these effects.

Vikuiti was defined using a native GEANT4 rough optical surface. Photons incident on the optical surface undergo specular lobe reflection with a spread parameterized by σ_α, which represents the width of a Gaussian distribution of surface micro-facet normals. Fiber collection efficiency was seen to not depend strongly on σ_α (Fig. 4). While the value of σ_α has not been experimentally measured, Vikuiti is known to not be a perfect specular reflector ($\sigma_\alpha > 0$). Due to the relative independence of light collection efficiency with σ_α, it is taken to be 3°, the median value between a perfect specular reflector and maximum efficiency, with $< 5\%$ uncertainty.

One method for increasing the fiber collection efficiency is to use higher concentration of the wavelength-shifting dye in the fibers. By concentrating the dye, the probability of a photon wavelength-shifting while

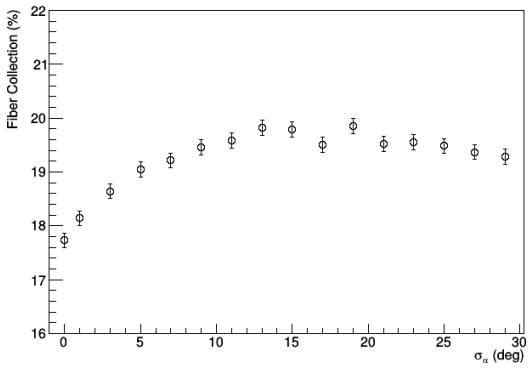

Figure 4. Fiber Light Collection Efficiency vs. Vikuiti Specularity

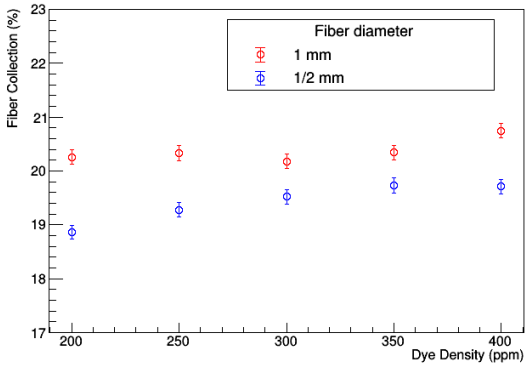

Figure 5. Light Collection Efficiency vs. WLS dye density and fiber diameter

traversing a fiber increases. This is tested in our simulation framework by scaling the wavelength-dependent absorption length of the fibers according to the dye density,

$$\lambda_a = \frac{1}{A_r(\lambda)\rho_d \ln 10}, \tag{2}$$

where $A_r(\lambda)$ is the absorbance and ρ_d is the dye density. The resulting simulations indicate that the fiber collection efficiency is only weakly dependent on the dye density in this light collection system, (Fig. 5) suggesting the fibers can be used at their nominal concentration of 200 ppm.

The impact of fiber diameter on collection efficiency was also investigated by simulating fiber geometries with diameters of ½ mm and 1 mm, both of which are available from Kuraray. Due to mechanical tolerances, the SiPMs should be somewhat larger than the clear fibers, which should in turn be somewhat larger than the WLS fibers. Larger differences ease mechanical tolerance requirements, but since the dark rate is proportional to sensor area the sensors cannot be made arbitrarily large. The chosen SiPMs are 1.3 mm on a side. The next-largest sensor is 3 mm on a side; five times the area and five times the dark rate. There is <10% performance difference for the different fiber diameters (Fig. 5) so ½ mm diameter was chosen to relax mechanical tolerances.

Another idea for increasing the collection efficiency is to embed the fibers in the acrylic of the cell walls. Embedding the fibers reduces the change in the index of refraction at the fiber/cell wall interface by eliminating the vacuum transition gap. This should decrease the number of photons that are prevented from reaching the fibers because of their total internal reflection off of this boundary.

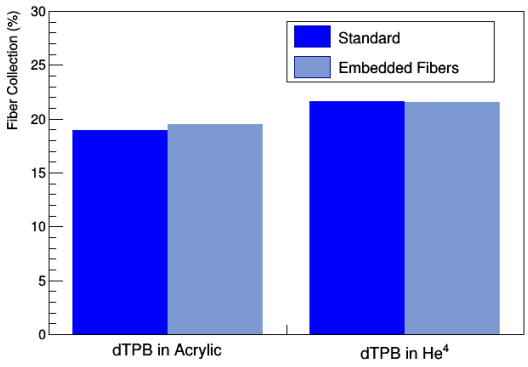

Figure 6. Fiber Light Collection Efficiency for embedded vs. unembedded fiber configurations. "dTPB in Acrylic" assumes that dTPB light is created inside the acrylic; "dTPB in 4He" assumes that dTPB light is created outside.

Fiber embedding was tested in two scenarios: with dTPB light produced in the acrylic on the measurement cell wall boundary and dTPB light produced outside of the acrylic (on the ^{4}He side of the boundary). As seen in Fig. 6, simulations show that embedding the fibers provides only slight improvement in light collection efficiency when the dTPB light is produced in the acrylic. Measurements of an early prototype of the nEDM@SNS light collection system found no captured light in the acrylic optical medium, suggesting that the light is primarily emitted in the dTPB outside the acrylic optical medium. In this case, the simulations indicate that the collection efficiency will be independent of the fiber embedding status.

B. UCN-^{3}He Capture Events

Our optimized geometry consists of 192 ½ mm diameter unembedded fibers with a 200 ppm dye density. Each fiber is looped into four adjacent segments along

the cell wall with both fiber ends read out by individual SiPMs, leading to 384 total SiPMs. σ_α for the Vikuiti VM2000 reflector film was set to 3°. Ito et al. [21] predict approximately 5050 primary UV photons from capture events when the electric field is 40 kV/cm. Taking the product of the efficiencies in Table 1, 3.25% of green photons produced in the WLS fibers will be transmitted to the SiPM readout. Thus, for this simulation

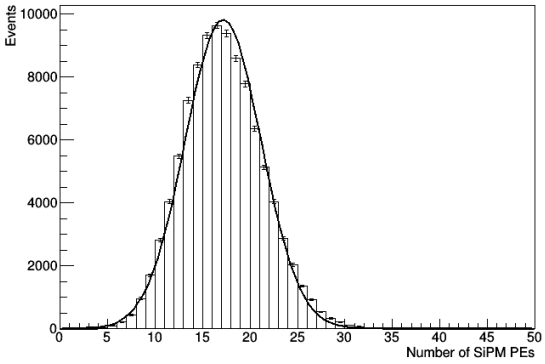

Figure 7. Number of photoelectrons detected in SiPMs from UCN-^{3}He capture events

which tracks only up until green photons are produced in the fibers, UCN-^{3}He capture events are simulated by emitting 163 ± 12.8 EUV photons from a capture event position into 4π. These photons then undergo the process laid out in Sec. II B. A simulation of 100,000 capture events emitted uniformly throughout the cell found the mean number of detected photoelectrons (NPE) to be 16.59 ± 4.14 per event (Fig. 7)

C. Event location reconstruction

Each readout channel (a group of 16 SiPMs) collects photons from fibers distributed over a strip of the cell wall limited to a 3.2 cm range in the beam direction. Thus, the distribution of hits binned by readout channel provides information on the event position in the beam direction. This information can be utilized to identify systematic effects and, as seen in Sec (III D), improve signal cuts that suppress experimental backgrounds.

Event position is calculated by the mean position of struck readout channels weighted by the NPE detected in each channel.

$$\bar{z} = \frac{\sum N_i z_i}{\sum N_i}. \tag{3}$$

At event positions near the cell windows ($|z| \gtrsim 15$), Eq. 3 is skewed by the asymmetric tail of the SiPM readout distribution towards the center of the cell. This

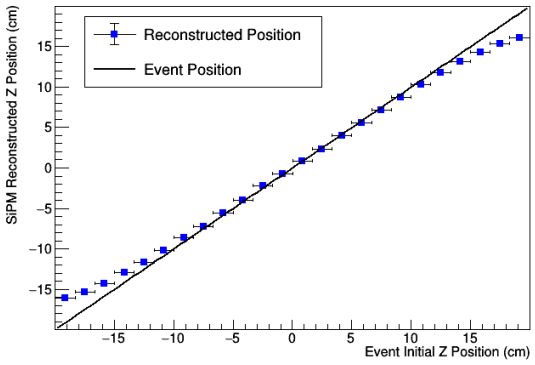

Figure 8. Reconstructed beam direction (z) location of UCN-^{3}He events using a truncated weighted mean of hit readout channel positions.

effect is reduced by implementing a truncation method, in which readout channels with 1 photoelectron are removed before the weighted mean is calculated (Fig. 8).

D. Background Suppressing Cuts

The primary source of background events is β-decay of the stored UCN, which produces an optical signal comparable to that of the UCN-^{3}He capture events. Background contributions from neutron activation, UCN wall loss, and cosmic rays are smaller and not studied here.

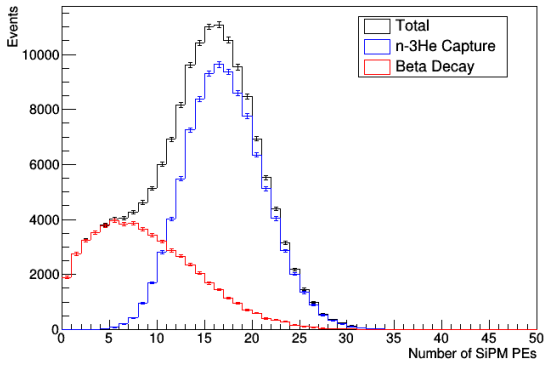

Figure 9. β decay background to the UCN-^{3}He capture signal.

β's are selected from the neutron β decay spectrum and simulated in the nEDM@SNS GEANT4 framework using a native scintillation process parameterized by the scintillation properties of liquid helium in a uniform electric field [9, 22]. The distribution of NPEs detected per event from neutron β decays is then normalized by

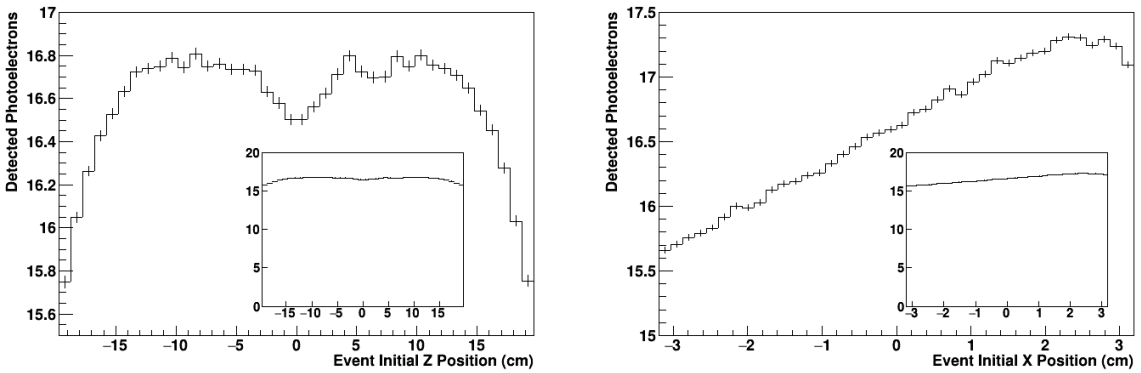

(a) (b)

Figure 10. ⟨NPE⟩ detected from UCN-^{3}He events (a) in the beam direction (b) in the plane perpendicular to beam and fibers (beam right). The insets show the plots without the suppressed zero in the y-axis, indicating the moderate impact of event position on ⟨NPE⟩.

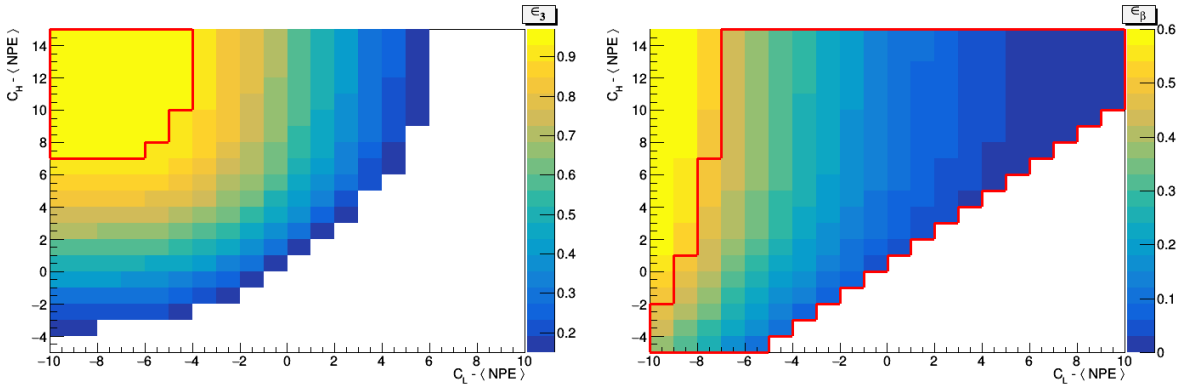

(a) (b)

Figure 11. Event detection efficiency across NPE cut parameter space for (a) UCN-^{3}He capture (b) β decay background. The region within the red contour in (a) satisfies $\epsilon_3 \geq 0.93$ and in (b) satisfies $\epsilon_\beta \leq 0.5$.

the ratio of the β decay rate to the capture rate at nominal wall loss, polarization loss, and ^{3}He density, $R_\beta/R_3 = 0.55$ [23] to produce Fig. 9.

In order to maximize signal sensitivity, the β-decay background (and other background sources with broad energy deposition distributions) can be suppressed via cuts on the NPE distribution relative to the expected yield from monoenergetic UCN-^{3}He capture events. The design goal of the nEDM@SNS experiment is to reduce the β decay background to 50% while maintaining 93% capture event detection efficiency. This can be accomplished with relatively narrow NPE cuts about the capture peak, with an especially narrow cut placed on the lower side of the capture peak where the β signal is concentrated. Asymmetric cuts about the capture peak, while minimizing the β signal, introduce position-dependent event detection efficiencies since the signal amplitude is modestly position-dependent along both the beam direction and the "beam right" direction (Fig. 10).

The dependence along the beam axis can be mitigated by using the reconstructed beam axis position (Sec. III C) to place z-dependent NPE cuts. Fig. 11 shows that to satisfy the design goals for the capture event detection efficiency, ϵ_3, and the β decay background detection efficiency ϵ_β with z-dependent NPE cuts, the acceptable region of the cut parameter-space ranges from $\langle\text{NPE}\rangle - 7 \leq \text{C}_\text{L} \leq \langle\text{NPE}\rangle - 5$ and $\langle\text{NPE}\rangle + 7 \leq \text{C}_\text{H} \leq \langle\text{NPE}\rangle + 14$, where $\langle\text{NPE}\rangle$ is the mean NPE for events within a 3.2 cm neighborhood of the event along the beam axis, and C_L, C_H are the low and high cuts on the NPE, respectively.

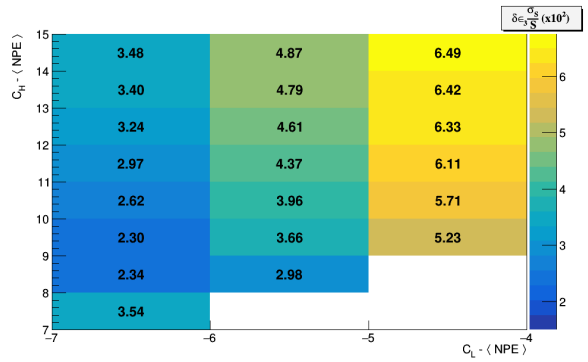

Figure 12. NPE cut placement optimization. The color scale is the product of variation in the signal detection efficiency ($\delta\epsilon_3$) and the relative error in the determination of the signal magnitude (σ_S/S).

On the other hand, the optical readout provides no information about the x position, so this effect can not be dealt with by placing position dependent cuts. Instead, it is addressed by using simulations to find the cuts that minimize the efficiency variance in the cut parameter-space region that satisfies the ϵ_3 and ϵ_β design goals. The efficiency variance across the measurement cell originates predominantly from two sources: the statistical error on the signal counts, σ_S/S (S = Total - Background), and the position-dependent variation induced by the asymmetric cuts, $\delta\epsilon_3$. In our simulation, the $\delta\epsilon_3$ is represented by the maximum difference in efficiencies across measurement cell positions from a specific cut. After normalizing $\delta\epsilon_3$ and σ_S/S with respect to one another, we find that the optimal cuts that minimize their product are placed at $C_L = \langle NPE \rangle - 7$ and $C_H = \langle NPE \rangle + 9$ (Fig. 12).

With NPE cuts placed at their optimal positions, the full event simulation was run with detected photoelectrons tagged by their corresponding event's reconstructed position. After making the position-dependent cuts, efficiencies ϵ_3 and ϵ_β were tabulated for events across the measurement cell. In all cases, the efficiencies meet their design goals ($\epsilon_3 \geq 0.93$, $\epsilon_\beta \leq 0.5$) with limited variations $\delta\epsilon_3$, $\delta\epsilon_\beta < 2\%$ (Fig. 13).

These efficiencies, ϵ_3 and ϵ_β, coupled with the sufficient value of $\langle NPE \rangle$ and small dependencies on the parameters addressed in these simulations inspire confidence that the current design of the light collection system can meet the stringent requirements of the experiment. Any uncertainty from the ad hoc inputs is addressed by using their worst case values, suggesting that these results provide a baseline that could potentially be improved upon. Additionally, an increase in the PDE, and thus the <NPE>, could be foreseen with improvements in SiPM devices in the forthcoming years. Although their contribution to the total background is less than β decay, a worthwhile extension to this study is properly modeling the effect of neutron activation and UCN wall loss on the signal detection efficiency and background rejection capability of the system.

IV. SUMMARY

The light collection system responsible for reading out the signal from UCN-^{3}He capture scintillation in the nEDM@SNS experiment has been designed and simulated. This system consists of a wavelength-shifting dTPB coating, a thin film dielectric reflector, wavelength-shifting optical fibers, and silicon photomultipliers.

Simulations indicate that previously untested parameters, such as fiber diameter, fiber dye density, fiber embedding, and thin film reflector surface roughness, have only minor effects on the final results. A mean of ~ 16 photoelectrons are detected per UCN-^{3}He capture event and the position of the event along the beam direction can be calculated to within several cm. Position-dependent cuts on the number of detected photoelectrons reduce the β decay background to sufficiently low levels. Additionally, the event position information can be used to identify further backgrounds/systematic effects. With optimized cuts, the efficiency of capture and β decay detection are uniform to $< 2\%$ across the measurement cell. These results hold promise for the successful implementation of the light collection system in the upcoming nEDM@SNS experiment. Construction of the system is underway and the system remains on track for installation into the experiment at a reasonable timeframe.

ACKNOWLEDGEMENTS

The authors would like to thank John Ramsey for the set of light collection system CAD models and Takeyasu Ito and Kent Leung for their support in the development of the light collection system simulation. The authors would also like to thank Leah Broussard, Bob Golub, Steve Lamoreaux, and Mike Hayden for their discussion and suggestions. This work was supported in part by the U.S. Department of Energy, Office of Science, Office of Workforce Development for Teachers and Scientists (WDTS) under the Science Undergraduate Laboratory Internship program.

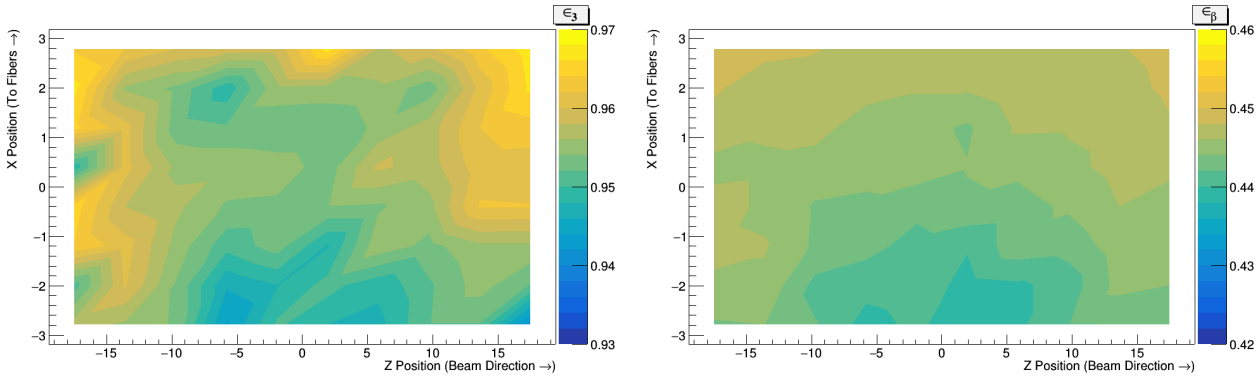

(a) (b)

Figure 13. Event detection efficiency throughout the measurement cell for (a) UCN-^{3}He capture (b) β decay background.

[1] M. W. Ahmed et al., "A New Cryogenic Apparatus to Search for the Neutron Electric Dipole Moment", J. Instrum. 14, P11017 (2019).

[2] R. Golub, S. Lamoreaux, "Neutron electric-dipole moment, ultracold neutrons and polarized ^{3}He", Phys. Rep. 237 (1994) 1

[3] C. Abel, et al., "Measurement of the Permanent Electric Dipole Moment of the Neutron", nEDM Collaboration, Phys. Rev. Lett. 124 (8) (2020) 081803,

[4] H. Fleishman and H. Einbinder and C.S. Wu, Scintillations from Liquid Helium, Rev. Sci. Instrum. 30, 1130 (1959).

[5] E.H. Thorndike and W.J. Shlaer, Scintillations from Liquid Helium, Rev. Sci. Instrum. 30, 838 (1959).

[6] D.N. McKinsey et al., "Detecting ionizing radiation in liquid helium using wavelength shifting light collection", Nucl. Instrum. Methods Phys. Res. Sect. A516, 475 (2004).

[7] Hamamatsu Photonics. Multi-Pixel Photon Counter Product Information. PDF. (2020).

[8] A.N. Otte et al. "Characterization of Three High Efficiency and Blue Sensitive Silicon Photomultipliers", Nucl. Instrum. Methods Phys. Res. A 846 (2017) 106-125

[9] D.N. McKinsey et al., "Time dependence of liquid-helium fluorescence", Phys. Rev. A67, 062716 (2003).

[10] K. Habicht, Ph.D. thesis, Technical University of Berlin, (1998).

[11] V.M. Gehman et al., "Characterization of protonated and deuterated Tetra-Phenyl Butadiene Film in a Polystyrene Matrix", J. Instrum. 8 P04024 (2013).

[12] S.K. Lamoreaux, ILL internal report 88LA0LT (1988).

[13] Q. Ye et al., "Relaxation of spin-polarized ^{3}He in mixtures of ^{3}He and ^{4}He at about 330 mK" Phys. Rev. A. 80, 023403 (2009).

[14] K.K.H. Leung, International Workshop: Probing Fundamental Symmetries and Interactions with UCN, 11-15 April 2016, JGU Mainz, Germany - Waldthausen Castle, `https://indico.mitp.uni-mainz.de/event/59/contributions/1992/attachments/1635/1713/4_Leung_Mainz.pdf`

[15] P. Gumplinger. "Optical Photon Processes in GEANT4", Users Workshop at CERN (2002).

[16] V.M. Gehman et al., "Fluorescence Efficiency and Visible Re-emission Spectrum of Tetraphenyl Butadiene Films at Extreme Ultraviolet Wavelengths", Nucl. Instrum. Meth. **A654**, 116 (2011).

[17] P. Mumm, private communication.

[18] Kuraray., Plastic Scintillating Fibers Catalogue, `https://www.kuraray.com/uploads/5a717515df6f5/PR0150_psf01.pdf`

[19] E.C. Dukes et al., "Performance of wavelength-shifting fibers for the Mu2e cosmic ray veto detector", J. Instrum. 13, P12028 (2018).

[20] Mitsubishi Chemical Corporation., Eska Polymer Optical Fiber Catalogue, `https://www.pofeska.com/pofeskae/product/01/index.html`

[21] T. M. Ito et al., "Effect of an electric field on superfluid helium scintillation produced by α-particle sources" Phys. Rev. A 85, 042718 (2012)

[22] N.S. Phan et al., "Effect of an electric field on liquid helium scintillation produced by fast electrons" arXiv:2005.03061 [physics.ins-det] (2020).

[23] K.K.H. Leung, private communication.